Chemisorption and Reactivity of Methanol on MgO Thin Films

Cristiana Di Valentin, Annalisa Del Vitto, and Gianfranco Pacchioni*

Dipartimento di Scienza dei Materiali, Università di Milano-Bicocca, and Istituto Nazionale per la Fisica della Materia, via R. Cozzi, 53 - I-20125 Milano, Italy

Stéphane Abbet, Anke S. Wörz, Ken Judai, and Ueli Heiz

Institute of Surface Chemistry and Catalysis, University of Ulm, D-89069 Ulm, Germany

Received: June 28, 2002; In Final Form: August 28, 2002

Methanol adsorption on MgO thin films has been studied by Fourier transform infrared (FTIR) and thermal desorption spectroscopies (TDS), and by ab initio cluster model calculations. Depending on the preparation conditions, films with various concentrations of defects have been obtained. These films exhibit different reactivity toward adsorbed methanol. In particular, at temperatures of 580 K, H_2 is released from defect-rich films while no production of hydrogen is observed on defect-poor films. The calculations show that methanol can interact in three different ways with the surface giving rise to physisorption, chemisorption, or heterolytic dissociation into CH_3O^- and H^+ fragments depending on the adsorption site. Chemisorption and dissociation occur only at defect sites, like low-coordinated ions at steps. Oxygen vacancies (F centers) are proposed as the sites present on the defect-rich films which are responsible for hydrogen release at high temperature.

1. Introduction

MgO is a typical basic oxide, which catalyzes the H_2 and D_2 exchange reactions[1] and the dehydrogenation of formic acid and methanol.[2] MgO is also used as a catalyst for the conversion of methanol and hydrogen sulfide into methanethiol and dimethyl sulfide.[3] In these processes it is assumed that methanol acts as a Broensted acid which dissociates heterolytically on the MgO surface via acid−base interactions, with formation of protons adsorbed on surface oxide anions.[1−3] Methanol has also been used as a probe molecule to study the adsorption sites on the MgO surface through the analysis of the IR frequencies.[4,5] The adsorption of methanol on polycrystalline MgO has been studied also with thermal desorption spectroscopies.[6]

The surface processes where methanol is adsorbed dissociatively are likely to involve defect sites more than the regular terraces. These sites can be low-coordinated ions, single or double vacancies, steps, or even impurity atoms.[7] The identification of the active sites of the MgO surface is therefore of crucial importance for the understanding of the reaction mechanisms and for the design of more efficient catalysts. In this respect, the possibility to grow thin oxide films in UHV on metal supports opens new perspectives to generate surfaces with controlled number and kind of defects.[8] Furthermore, it also allows one to use electron spectroscopies for the structural and electronic characterization of the surface.[9,10] In this respect, methanol has been used to check the reactivity of MgO ultrathin films.[11−13] However, these preparation methods alone do not guarantee a complete control on nature and concentration of active sites on the surface. The knowledge of the defect sites which are present on the surface is still limited. Some progress in this direction becomes possible when the experimental data on adsorption and reactivity of a given species are compared with the predictions of first principles calculations on a structural model of the active site.[7] This approach has led in the past few years to a considerable advance in mapping the MgO surface sites which are responsible for part of its chemistry.[14−16]

In this paper, we present a combined theoretical−experimental study aimed at a better characterization of the morphology of the MgO surface. Ultrathin MgO films of 10 monolayers thickness have been grown on a Mo(100) substrate under various conditions. The films show a different number of defect sites and can be classified as defect-rich and defect-poor films, respectively. Their reaction with methanol is then studied through Fourier transform infrared (FTIR) and thermal desorption spectroscopy (TDS) measurements of the adsorbed species. Structural models of the active sites are designed and their properties are computed with accurate ab initio embedded cluster calculations. The computed IR spectra and desorption energies are compared with the measured ones. We will show that the observed reactivity of the defect-rich films is consistent with the existence of neutral oxygen vacancies,[17] or F centers.

The paper is organized as follows. After a description of the experimental (Section 2) and theoretical (Section 3) details, we discuss the TDS and FTIR results in Section 4 and the cluster calculations in Section 5. In Section 6 we present a discussion where the experimental and the theoretical data are compared and related to other literature data. This allows us to draw some general conclusions about the sites involved in the reactivity of methanol with the MgO thin films. The conclusions are briefly summarized in Section 7.

2. Experimental Method

The adsorption of methanol was studied experimentally on well-characterized thin films of MgO(100). They are grown on Mo(100) single crystals by evaporating pure metallic magnesium in an oxygen background of 1×10^{-6} mbar. Subsequently they are annealed to 840 K. Auger electron spectroscopy (AES) measurements show a one-to-one stoichiometry of the films and the absence of any impurity.[18] Typical thicknesses were about

* Corresponding author. E-mail: gianfranco.pacchioni@unimib.it

10.1021/jp026399q CCC: $22.00
Published on Web 10/25/2002

10 monolayers, as determined by AES peak intensities and by X-ray photoemission (XPS) using the intensity attenuation of the Mo 3d core level with increasing film coverage.[19]

Low-energy electron diffraction (LEED) of a MgO film after a short annealing shows a sharp (1 × 1) pattern.[19] Multiple phonon losses in the high-resolution electron energy loss spectrum (HREELS), the characteristic UPS from the O 2p valence band, and electron energy loss spectra (EELS) with the characteristic loss at about 6 eV[19] indicate a well-ordered MgO-(100) single-crystal surface in good agreement with previous studies.[20−24]

Although these MgO(100) films reveal properties similar to those observed for the corresponding three-dimensional solids, they expose, depending on the Mg evaporation rate (defect-poor: 0.5 ML/min; defect-rich: 5 ML/min), O_2 background pressure (defect-poor: 5×10^{-7} mbar; defect-rich: 1×10^{-6} mbar), and annealing temperature (840 K), a reproducible density of defects on their surface. These defects are characterized by the adsorption properties of small molecules. For CO chemisorption on MgO(100) it was concluded from highly accurate first-principle theoretical model calculations[25] that the relatively strong chemisorption energy coupled with an unusual blue-shift of the CO frequency in CO/MgO(100)/Mo(100) reported experimentally[26] cannot correspond to chemisorption on regular, unperturbed, five-coordinated sites as claimed.[27,28] Rather, it was suggested that the unusually strong interaction should be connected with extended defects (steps, kinks) on the oxide film. In addition to the extended defect sites, oxygen vacancies (F-centers) could be detected.[14] The existence of F-centers is deduced from the good agreement of experimental and theoretical binding energies and vibrational frequencies of CO adsorbed to single Pd atoms trapped on the point defects. STM measurements of a 2 ML MgO/Ag(001) thin film, epitaxially grown at 500 K, also point to the existence of F-centers.[14]

The in-situ prepared films were then exposed to 6 Langmuir of methanol by backfilling the UHV system (1 L = 1×10^6 Torr s) and the adsorption was characterized by using TDS, Figure 1, and FTIR spectroscopies, Figures 1 and 2. For the TDS experiments a heating rate of 2 K/s was used and the desorbing molecule was detected with a differentially pumped mass spectrometer (Balzers QMS 420) after electron impact (70 eV) ionization. To prevent electron-stimulated processes the sample was protected by a biased (−150 V) skimmer with an orifice of 3 mm; this excludes the detection of negatively charged desorbing molecules. The infrared spectra were measured in single reflection mode where the infrared beam is focused at grazing angle (85°) onto the sample. The reflected beam was detected by a narrow band MCT detector. A total of 512 interferograms were averaged, and no smoothing of the spectra was performed.

3. Computational Method

The interaction of a CH_3OH molecule with the MgO(100) surface has been modeled by finite stoichiometric MgO clusters embedded in ±2 point charges (PC). Various adsorption sites have been considered: regular (100) terrace sites, low coordinated ions (i.e., edge or step sites), and neutral oxygen vacancies. These latter centers consists of the cavity left by the missing anion and are characterized by the presence of two trapped electrons which are responsible for a characteristic reactivity of the defect.[17]

The truncation of the lattice in cluster models of ionic materials implies the use of external fields to represent the long-range Coulomb potential.[29] We used a large array of PCs to reproduce the Madelung potential at the adsorption site. A disadvantage of this technique is that the PCs induce an artificial polarization of the O^{2-} anions at the cluster border, which causes an incorrect behavior of the electrostatic potential in the adsorption region. This problem can be circumvented by placing effective core potentials (ECPs)[30,31] instead of positive PCs at the cluster borders.[32−34] The ECP, providing a representation of the finite size of the cation, essentially removes the artificial polarization of the O^{2-} electron cloud. This model has been successfully applied in a variety of cases and compared with more elaborated embedding schemes as well as with periodic calculations.[35] From all these comparisons, the robustness of the approach has been carefully verified over the years.[7,36]

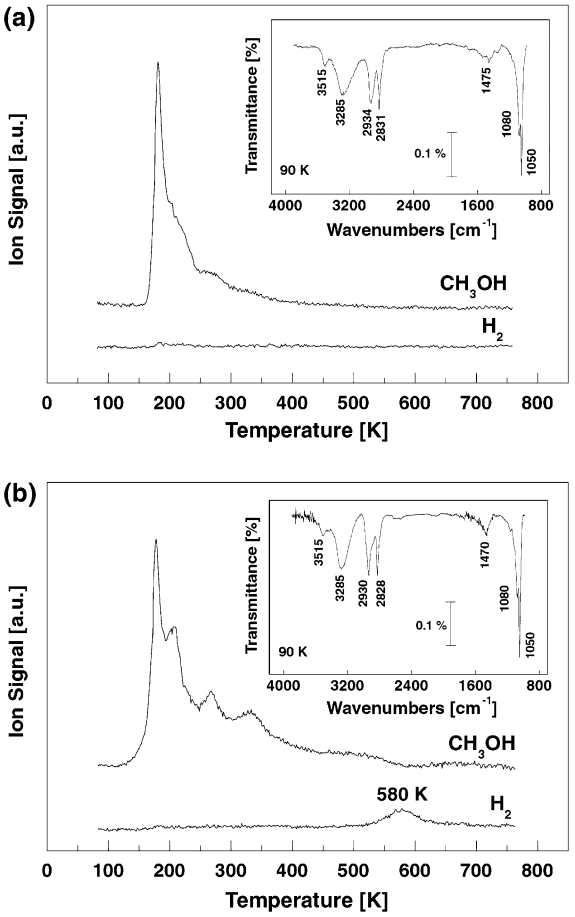

Figure 1. Thermal desorption spectra of CH_3OH and H_2 on (a) defect-poor MgO(100)/Mo(100) thin films, and (b) defect-rich MgO(100)/Mo(100) thin films after a dosage of about 6 L of CH_3OH at 90 K. Note that desorption of H_2 at 580 K is observed only on defect-rich thin films. The inserts report FTIR spectra recorded at 90 K after dosage of about 6 L of CH_3OH on (a) defect-poor MgO(100)/Mo(100) thin films, and (b) defect-rich MgO(100)/Mo(100) thin films. No remarkable differences are observed between the two FTIR spectra.

The MgO(100) terraces have been modeled by two different clusters: a $[Mg_8O_8ECP_{14}]$ cluster surrounded by 698 PCs, Figure 3a, and a $[Mg_{18}O_{18}ECP_{23}]$ cluster surrounded by 669 PCs, Figure 3b,c. For the edge site we have used a $[Mg_8O_8ECP_{12}]$ cluster surrounded by 658 PCs, Figure 4a,b and a $[Mg_{11}O_{11}ECP_{12}]$ cluster surrounded by 652 PCs, Figure 4c, respectively. For the model of a step site we have used a $[Mg_{15}O_{15}ECP_{18}]$ cluster surrounded by 550 PCs, Figure 5. All clusters used are centered on a Mg−O pair of atoms. The models of F_S centers have been obtained by removing an O atom from corresponding models of terrace and edge sites: $[Mg_{18}O_{17}ECP_{23}]$ for a terrace F_S

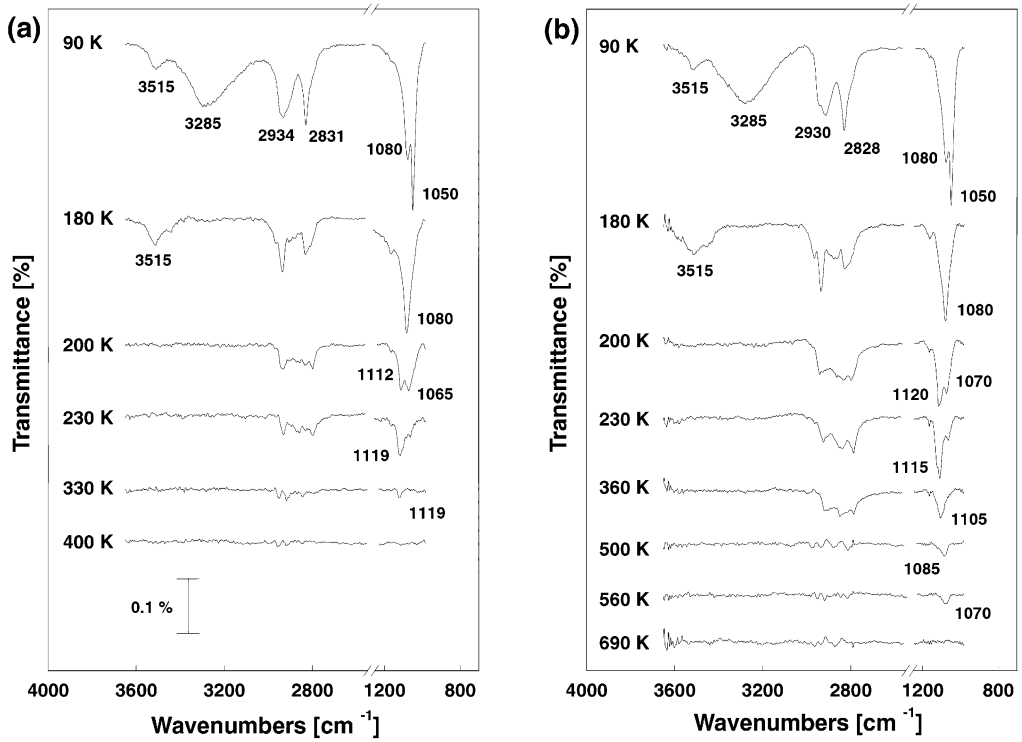

Figure 2. Thermal evolution of FTIR spectra measured at 90 K and after annealing the sample to the indicated temperature. Shown are the regions between 3650−2550 cm^{-1} and 1250−980 cm^{-1} (dosage: 6 L of CH_3OH at 90 K). On defect-poor MgO(100)/Mo(100) thin films (a), the evolution is shown up to 400 K. At this temperature, no absorption bands are observed. On defect-rich MgO(100)/Mo(100) thin films (b), the spectra are shown up to 690 K.

center, Figure 6, and $[Mg_{11}O_{10}ECP_{12}]$ for an equivalent edge center, Figure 7a,b.

The calculations were performed at the density functional theory (DFT) level using the gradient-corrected Becke's three parameters hybrid exchange functional[37] in combination with the correlation functional of Lee, Yang, and Parr,[38] generally referred to as B3LYP. It has been shown that this functional provides the best results in terms of chemical accuracy.[39]

Geometry optimizations were performed by means of analytical gradients with no symmetry constraints. We started by optimizing the smaller clusters where only the central pair of Mg and O atoms were free to relax. On the larger clusters, all the Mg and O ions nearest neighbors of the adsorption sites (or of the oxygen vacancy) were allowed to relax. Vibrational frequencies have been computed by determining the second derivatives of the total energy with respect to the internal coordinates. To reduce the computational effort, some of the vibrational analyses have been performed on smaller clusters which, however, properly represent the vibrations of the adsorbed system.

The 6-31G*[35] basis set was used for the Mg and O ions directly interacting with adsorbed species or for the Mg cations surrounding the oxygen vacancy. The remaining Mg and O ions have been treated with a 6-31G basis set. The C, O, and H atoms of CH_3OH were described with the 6-31+G** basis set.[40] In the calculation of the oxygen vacancies, no floating functions have been placed at the center of the vacancy.[35] The binding energies have been corrected by the basis set superposition error (BSSE) using the counter-poise correction.[41] The calculations have been performed using the Gaussian-98 program package.[42]

4. Experimental Section Results

The interaction of methanol with the defect-poor and defect-rich films was first studied using TDS (Figure 1a,b). For both films the desorption of physisorbed methanol at around 180 K is most dominant. On the defect-poor films, small amounts of chemisorbed methanol desorb up to around 350 K. On defect-rich films, the desorption of chemisorbed methanol evolves in three distinct peaks at 200, 260, and 340 K. A small reproducible feature is observed at around 500 K. The corresponding infrared spectra taken at 90 K (insets of Figure 1a,b) confirm the presence of mainly physisorbed CH_3OH with a typical band for the OH-group at 3285 cm^{-1}, bands of the symmetric stretch (2930 cm^{-1}/2828 cm^{-1}), and the bending (1475 cm^{-1}) modes of the CH_3 group and the C−O vibrational mode at 1080 cm^{-1}. To better characterize the adsorbed methanol species, the infrared spectra were taken as a function of annealing temperature (Figure 2a,b). In these experiments the sample was flashed to the indicated temperature and the spectra were recorded at 90 K. For defect-poor films, most of the intensity of the vibrational bands disappear between 180 and 200 K, consistent with the desorption observed at 180 K in the TDS (Figure 2a). Up to temperatures of about 400 K, small bands are observed for the CH_3− and C−O bands. Their intensity is decreasing with temperature. These bands are attributed to chemisorbed methanol. As for the defect-rich films, the evolution of the IR-spectra with temperature is consistent with the corresponding TDS. Physisorbed methanol desorbs before 200 K (disappearance of the OH-band), and the more intense vibrational features of chemisorbed methanol are unambiguously detected up to 360 K. At higher temperatures, a clear peak is observed at 1070−1085 cm^{-1} and in the range of the CH_3 stretch modes, which are slightly shifted to the blue. It is difficult, however, to distinguish these latter features from the background, especially those at 690 K we attribute to noise in the background spectrum. It is interesting to note that the disappearance of the band at 1070 cm^{-1} correlates with the desorption of H_2 from the surface, and

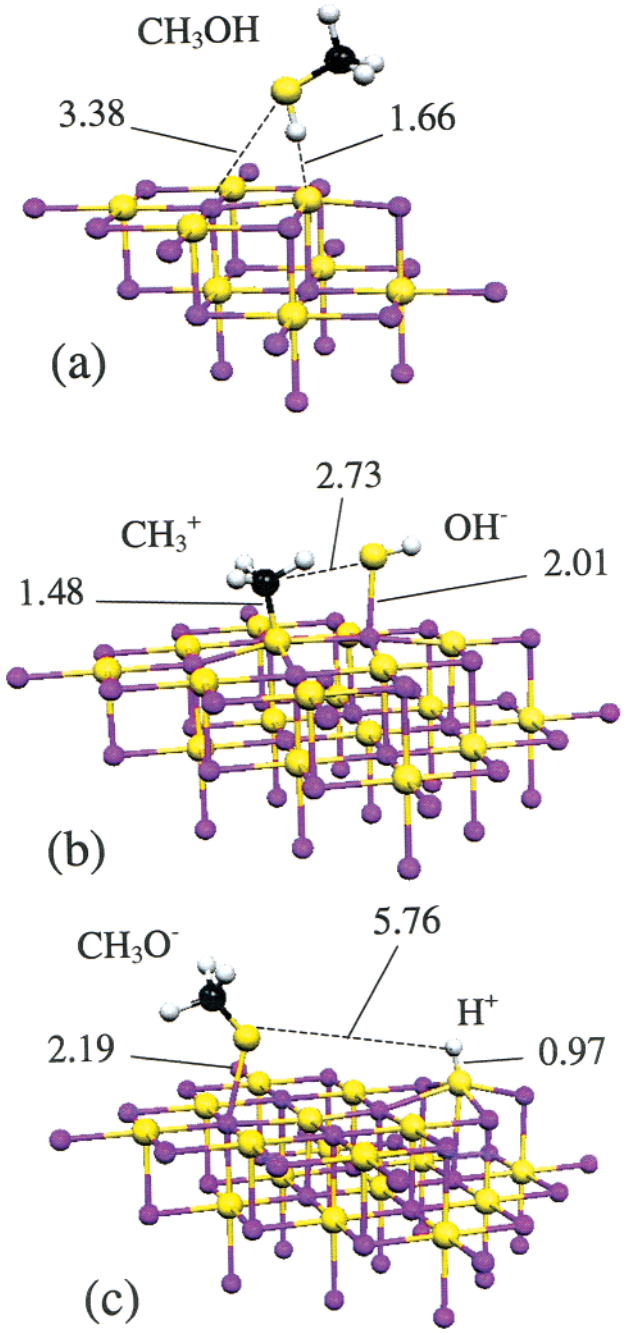

Figure 3. Model of a non-defective terrace site. (a) Physisorbed CH_3OH on $[O_8Mg_8ECP_{14}]$; (b) chemisorbed CH_3OH ($CH_3^+-OH^-$) on $[O_{18}Mg_{18}ECP_{23}]$; (c) dissociated CH_3OH ($CH_3O^- + H^+$) on $[O_{18}Mg_{18}ECP_{23}]$. Small magenta spheres: Mg; large yellow spheres: O. Selected distances in Å. The Mg ions treated with ECPs are those at larger distance from the Mg−O adsorption site.

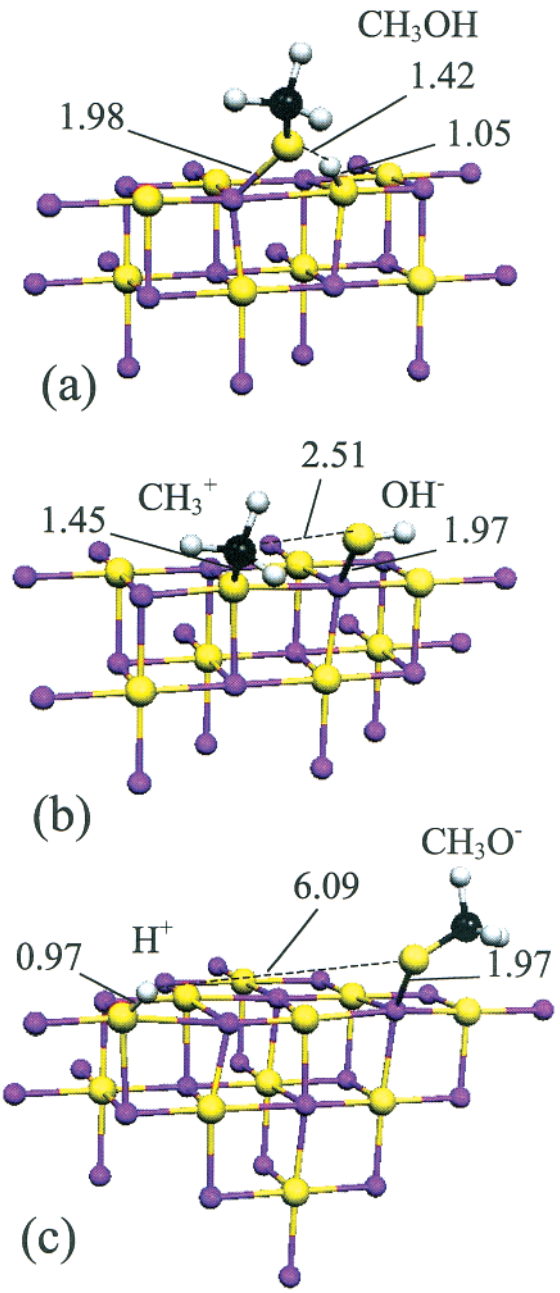

Figure 4. Model of an edge site. (a) Chemisorbed CH_3OH ($CH_3O^- - H^+$) on $[O_8Mg_8ECP_{12}]$; (b) chemisorbed CH_3OH ($CH_3^+-OH^-$) on $[O_8Mg_8ECP_{12}]$; (c) dissociated CH_3OH ($CH_3O^- + H^+$) on $[O_{11}Mg_{11}ECP_{12}]$. For definitions, see Figure 3.

therefore we attribute this peak to a proton trapped in the cavity of an F-center (see discussion).

5. Computational Results

MgO is a basic oxide characterized by a large charge separation of the constituting ions. This means that strong electric fields are experienced by adsorbed molecules when they approach the surface. This may result in heterolytic splitting of covalent bonds, as is the case for the H_2 or H_2O molecules.[43,44] Water dissociation on MgO has been the subject of several studies. For a long time it was believed that only low-coordinated sites are able to dissociate water,[45] but recently it has been predicted theoretically that in the presence of an overlayer of water also dissociation at (100) MgO terraces is possible,[46] a result which has been confirmed experimentally.[47] However, this form of dissociated water exists only in the low-temperature regime, while dissociation at steps and corners leads to the formation of stable hydroxyl groups. It has been suggested that a similar process occurs for methanol.[12] Therefore, we first computed the energy cost for heterolytic breaking of methanol in the gas phase to give charged fragments (ΔE is the reaction energy and is defined positive for an endothermic reaction):

$$CH_3OH_{(g)} \rightarrow CH_3O^-_{(g)} + H^+_{(g)} \quad \Delta E = +16.9 \text{ eV} \quad (1)$$

$$CH_3OH_{(g)} \rightarrow CH_3^+{}_{(g)} + OH^-_{(g)} \quad \Delta E = +12.1 \text{ eV} \quad (2)$$

Not surprisingly, these energies are very high, much higher than

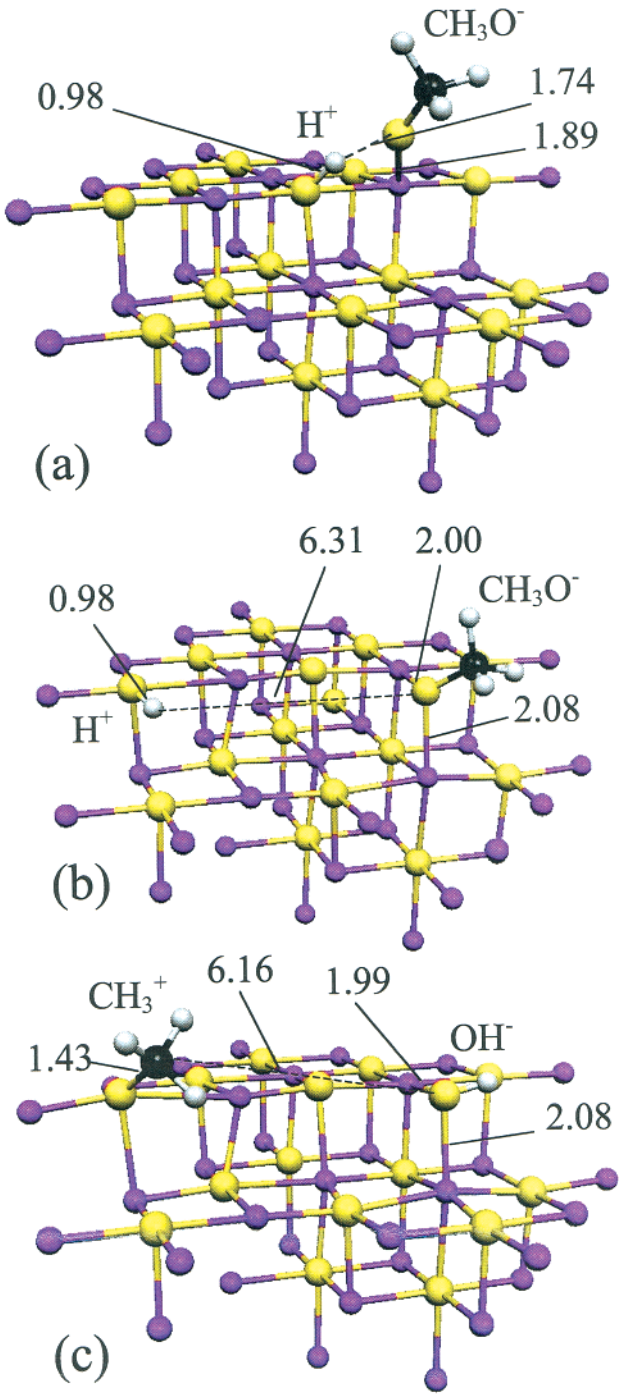

Figure 5. Model of a step site. (a) Chemisorbed CH_3OH ($CH_3O^- - H^+$) on [$O_{15}Mg_{15}ECP_{18}$]; (b) dissociated CH_3OH ($CH_3O^- + H^+$) on [$O_{15}Mg_{15}ECP_{18}$]; (c) dissociated CH_3OH ($CH_3^+ + OH^-$) on [$O_{15}Mg_{15}ECP_{18}$]. For definitions, see Figure 3.

those required for homolytic dissociation (radical mechanism):

$$CH_3OH_{(g)} \rightarrow CH_3O^{\cdot}_{(g)} + H^{\cdot}_{(g)} \quad \Delta E = +4.1 \text{ eV} \qquad (3)$$

$$CH_3OH_{(g)} \rightarrow CH_3^{\cdot}{}_{(g)} + OH^{\cdot}_{(g)} \quad \Delta E = +4.7 \text{ eV} \qquad (4)$$

Clearly, the situation can be quite different on the surface where charged fragments can be stabilized at the cation or anion sites of the MgO surface.

The calculations show that the adsorption of methanol on MgO leads to a variety of situations, strongly dependent on the adsorption site. This can provide a way to characterize the

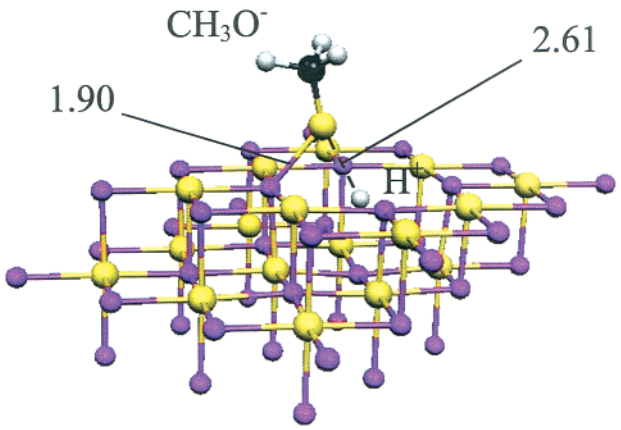

Figure 6. Model of an oxygen vacancy at a terrace. Chemisorbed CH_3OH ($CH_3O^- - H^+$) on [$O_{17}Mg_{18}ECP_{23}$]. For definitions, see Figure 3.

TABLE 1: Energetics of Methanol Adsorption at Various Sites of the MgO Surface[a]

cluster	site	adsorption mode	ΔE (eV) (BSSE)[b]
[$Mg_8O_8ECP_{12}$]	terrace	physisorbed	−0.54 (−0.43)
[$Mg_{18}O_{18}ECP_{23}$]		chemisorbed $CH_3^+ - OH^-$	+1.00
		dissociated $CH_3O^- + H^+$	+2.80
[$Mg_{11}O_{11}ECP_{12}$]	edge	chemisorbed $CH_3O^- - H^+$	−1.06 (−0.85)
		chemisorbed $CH_3^+ - OH^-$	+0.23
		dissociated $CH_3O^- + H^+$	+1.68
[$Mg_{15}O_{15}ECP_{18}$]	step	chemisorbed $CH_3O^- - H^+$	−1.77
		dissociated $CH_3O^- + H^+$	−0.16
		dissociated $CH_3^+ + OH^-$	+0.01
[$Mg_{18}O_{17}ECP_{23}$]	terrace F_S	dissociated $CH_3O^- + H^+$	−2.33
[$Mg_{11}O_{10}ECP_{12}$]	edge F_S	chemisorbed $CH_3O^- - H^+$	−2.17
		dissociated $CH_3O^- + H^+$	+0.94

[a] Negative values correspond to exothermic adsorption. [b] BSSE values in parentheses.

surface heterogeneity and morphology. In general, one can identify three different interaction modes for methanol adsorbed on MgO. In the following we refer to these bonding modes as (i) physisorption, (ii) chemisorption, and (iii) dissociative adsorption. The first case, (i), corresponds to a weak interaction, dominated by electrostatic or dispersion forces and small modifications of the molecular structure; in (ii) the molecule is more strongly bound, considerably activated so that weakly interacting molecular fragments can be identified (however, the bonds are not completely broken); in the last case (iii), the bonds between the fragments are completely broken and the two species sit on different adsorption sites on the surface. What determines one adsorption mode or the other is the electronic nature of the site where the interaction occurs. Therefore, in the following we analyze the various adsorption modes which originate from the interaction of methanol with the surface.

5.1. Terrace Sites. We consider first methanol adsorption on a nondefective (100) terrace. Here the isolated molecule is physisorbed with a energy gain of 0.54 eV, a value which is reduced to 0.43 eV after BSSE correction, Table 1. The molecule is practically undistorted compared to the gas phase, Figure 3a, in agreement with other recent ab initio calculations done on bare MgO clusters.[48] Thus, on the MgO flat terraces neither chemisorption nor dissociation occurs. This has been checked by adsorbing separately the products of reaction 1. When the CH_3O^- and H^+ fragments are placed at a short distance on the same cluster, the geometry optimization results in a spontaneous recombination and formation of a physisorbed CH_3OH species. Starting from the products of reaction 2, CH_3^+ and OH^-, adsorbed on a pair of adjacent O^{2-} and Mg^{2+} ions, the geometry optimization leads to a local minimum, Figure 3b, which lies

1.00 eV above the energy of the reactants, $MgO_{(s)} + CH_3OH_{(g)}$, Table 1. Thus the heterolytic dissociation (reaction 2) is endothermic and a barrier (not investigated here) separates the fragments from the noninteracting units. We also considered the possibility of having dissociated fragments at a longer distance in order to evaluate the cost of the dissociation (reaction 1) on the surface. For this calculation, we used the $[Mg_{18}O_{18}ECP_{23}]$ cluster and we placed the CH_3O^- and H^+ adsorbed fragments 6.3 Å apart. The geometry optimization results in a local minimum, Figure 3c, which is 2.80 eV higher than the reactants.

The adsorption energy of the isolated ionic fragments (i.e., at infinite distance) can be evaluated by placing them on different clusters, Mg_8O_8 and O_8Mg_8. CH_3O^- is bound to Mg^{2+} by 0.54 eV only, while the binding of H^+ to an O^{2-} ion is 11.55 eV (values not corrected by the BSSE). Therefore, the total energy gain when CH_3O^- and H^+ ionic fragments are adsorbed on MgO is estimated to be −12.1 eV, which has to be compared with the 16.9 eV cost to heterolytically dissociate methanol in the gas phase (the total cost for reaction 1 is thus +4.8 eV). Of course, on the surface there is an additional electrostatic interaction of the two ionic adsorbates which lowers the energy; in fact, in our calculation where the two fragments are initially placed 6.3 Å apart, the total cost for dissociation is of 2.8 eV and the electrostatic interaction contributes about 2 eV. In any case, on the terrace sites, reaction 1 is endothermic. This analysis has been repeated for reaction 2 by adsorbing the ionic fragments on two different clusters, Mg_8O_8 and O_8Mg_8. CH_3^+ is bound to O^{2-} by 6.4 eV, while OH^- is bound to Mg^{2+} by 0.5 eV; the total energy gain is 6.9 eV, again much too low to compensate for the 12.1 eV cost to dissociate methanol according to reaction 2.

The results show that on the terrace sites, which are the most abundant on the thin MgO films, only physisorption takes place. This means that for temperatures above liquid nitrogen only a small fraction of the adsorbed species will survive, and in particular only those molecules which have reacted with irregular sites.

5.2. Edge or Step Sites. It is well-known that the reactivity of MgO is considerably enhanced on low-coordinated sites or other point defects.[7] Therefore, it is not surprising that when methanol is adsorbed on a MgO edge or step, physisorption is not observed. Rather, we found a strong elongation of the O−H bond which leads to a chemisorbed methanol molecule, $CH_3O^-{-}H^+$, Figure 4a. The species is now bound by 1.06 eV (0.85 eV with the BSSE), Table 1, with respect to the noninteracting units but dissociation has not occurred since the O−H bond is elongated to 1.45 Å but is not completely broken, Figure 4a. For comparison, the same distance in $CH_3OH_{(g)}$ is 0.97 Å. The formation of the chemisorbed species is nonactivated as it does not imply to overcome an activation barrier. Optimizing the geometry from a different starting point where the two ionic fragments of reaction 2, CH_3^+ and OH^-, are placed above two neighboring Mg and O anions at an edge site, we observe the formation of a chemisorbed complex with an elongated C−O bond, 2.5 Å (1.4 Å in the gas phase), Figure 4b; the reaction is slightly endothermic, by 0.23 eV, Table 1. Thus, on the more reactive edge sites activation of methanol bonds is possible, but without complete dissociation. In fact, when we put the two species, CH_3O^- and H^+, at a distance of 6.3 Å on $[Mg_{11}O_{11}ECP_{12}]$ and we optimize the structure, we end up in a local minimum, Figure 4c, which is 1.68 eV higher than $MgO_{(s)} + CH_3OH_{(g)}$. Since the chemisorbed molecule is bound by 1.1 eV, it follows that the separation of the two ionic fragments on the edge has an energy cost of 2.8 eV due to the electrostatic interaction of the two charged species. This is confirmed by the data obtained by placing the two fragments on isolated models of Mg^{2+} cations or O^{2-} anions on edge sites (Mg_8O_8 and O_8Mg_8 clusters, respectively): the CH_3O^- binding energy is 0.75 eV, while that for H^+ is 11.8 eV, with only a moderate increase with respect to the terrace sites. The complete dissociation process (reaction 1) requires therefore 4.25 eV to take place on edges. The same holds for dissociation (reaction 2): when the two isolated species, CH_3^+ and OH^-, are placed on models of edge sites they are stabilized by 6.7 and 0.9 eV, respectively, with a cost for dissociation of 4.8 eV. Notice that while on terraces, reaction 1 is preferred over reaction 2 by 2 eV; on edge sites, the difference in favor of (reaction 1) is reduced to 0.55 eV.

So far we have considered only models of edge sites, originating from the intersection of two extended (100) faces. Much more common on the surface are the step defects. We have modeled methanol adsorption on a step by means of the $[Mg_{15}O_{15}ECP_{18}]$ cluster, Figure 5. On this site, methanol chemisorption is even more favorable than on an edge site, with an energy gain close to 1.77 eV, Table 1 and Figure 5a. Interestingly, on this site dissociation (reaction 1) is exothermic, even when the two fragments are relatively far apart: the optimal structure obtained starting from the two species, CH_3O^- and H^+ species 6.3 Å apart, Figure 5b, is 0.16 eV more stable than the reactants. Even the dissociation on CH_3^+ and OH^- fragments is possible as the calculations show a thermoneutral reaction for this process on a step, Table 1 and Figure 5c. The slight preference for dissociation (reaction 1) is sufficient to obtain almost exclusively this state; however, it is not excluded that under some conditions reaction 2 can also take place in small amounts.

In this study we have not considered other low-coordinated sites such as three-coordinated ions at kinks and corners; these are known to be chemically very active and to promote the dissociation of molecules which do not react on other sites such as edges and steps.[49,50] It is possible that these sites will dissociate methanol. However, the number of three-coordinated sites should be comparatively small in MgO(100) films.

To summarize, on edge MgO pairs the complete dissociation of methanol molecules is endothermic, while chemisorption accompanied by partial activation is a spontaneous process with a gain of 1.06 eV; on a step even the complete dissociation is slightly exothermic. These results suggest that methanol desorption from edge or step sites should occur by recombination of the two fragments around or slightly below room temperature.

5.3. F_s Centers. The results presented above do not completely account for some of the experimental observations (Section 4). In particular, the formation of molecular H_2 from the surface at 580 K is not easily accounted for in the frame of the adsorption modes of methanol on edge or step sites. Hydrogen desorption could in principle involve the methyl groups of the methanol molecule. IR studies performed on polycrystalline MgO using both CH_3OH and CD_3OH species[5] have suggested the occurrence of some exchange reactions involving hydrogen at elevated temperatures, $T > 650$ K. From the above analysis, we have seen that formation of CH_3 fragments is generally less favorable than that of OCH_3 units. Therefore, if methyl groups and their dissociation are involved in the hydrogen release, this should be a minority channel reaction. The occurrence of hydrogen exchange during methanol adsorption has not been reported in more recent studies.

One aspect which has not been considered so far in the discussion of the surface reactivity of MgO toward methanol is

TABLE 2: Selected Frequencies, in cm^{-1}, Computed at the B3LYP Level for Adsorbed Methanol

system	site	cluster	ν(OH)	ν(CH)	δ(CH)	δ(OH)	ν(CO)	ν(MgH)
CH_3OH physisorbed	terrace	$O_8Mg_8ECP_{14}$	3102	2946 2978 3065	1547	1478	1087	
CH_3O^-	step	$O_8Mg_2ECP_{18}$		2462 2681 2882	1421 1459 1493	1180	1145	
OH^-	edge	$O_8Mg_8ECP_{12}$	3681	-	-		-	
CH_3^+	edge	O_1Mg_4		2987 3047 3099	1497 1521 1543	1157 1203	992	
CH_3O^-	F center terrace	$O_{17}Mg_{18}ECP_{23}$		2874 2894 2902	1480		1083	
proton	F center terrace	$O_{17}Mg_{18}ECP_{23}$						920 1030

the role of oxygen vacancies. These defect centers are known to play an important role on the surface properties of MgO in general[7,16] and of MgO thin films in particular.[14] The presence and the nature of F centers at the surface of MgO is now quite well established.[7] Therefore, we consider here the interaction of CH_3OH with these highly reactive centers.

Methanol initially physisorbs on a terrace F_S center with a binding of 0.27 eV; in this structure the O atom of methanol is 2.7 Å from one Mg^{2+} cation of the vacancy with the proton oriented toward the cavity (this minimum could also be due to the occurrence of the BSSE). This precursor evolves into the chemisorbed state, Figure 6, by reducing the distance from the surface. In this structure, the CH_3O^- fragment is bound to a Mg^{2+} cation around the cavity, while the proton is completely introduced in the vacancy and surrounded by the two electrons. Notice that, formally, one proton surrounded by two electrons corresponds to an hydride ion, H^-. The O−H distance is elongated to 2.1 Å, a value which indicates nearly complete dissociation. The structure is 2.33 eV more stable than the reactants, thus confirming the high reactivity of these centers (giving the high stabilization, no BSSE correction has been introduced here).

Oxygen vacancies can also form along step edges of the surface, and in fact theoretical studies show that the formation energy of an F center is lower for low-coordinated oxygen atoms.[51] Thus, we have considered an oxygen vacancy at an edge site, Figure 7: here methanol is bound by 2.17 eV and the O−H distance, 2.6 Å, Figure 7a, is even longer than on a terrace F center. Also in this case, however, the role of the short-range electrostatic interaction is crucial. In fact, if we put the two ionic fragments at a longer distance, 6.3 Å, see Figure 7b, the ΔE of the reaction becomes positive (endothermic) by about 1 eV. Thus, it is likely that migration of CH_3O^- or H^+ species on the surface is possible only at temperatures well above RT.

5.4. IR Frequencies. We have calculated the harmonic IR frequencies of some of the species investigated above, either in physisorbed or chemisorbed form. We also considered the vibrational frequencies of the isolated products of reactions 1 and 2. The frequencies, calculated at 0 K, are reported in Table 2.

To check the reliability of our IR results, we first computed the IR frequencies for gas-phase CH_3OH (in parentheses are the experimental ones[52]): 3842 cm^{-1} for ν(OH) (3682 cm^{-1}), 3100 cm^{-1} for ν(CH) (2844 cm^{-1}), 1050 cm^{-1} for ν(CO) (1034 cm^{-1}), and 1500 cm^{-1} δ(OCH) (1340 cm^{-1}). The highest frequency for the O−H and C−H stretchings is overestimated by about 5%; the C−O stretching, on the contrary, is quite close to the experimental one. The application of a scaling factor would bring the high-energy vibrations in closer contact with the experiment at the cost of reducing the accuracy for the low-frequency region. Since this latter region is the more interesting one from the point of view of the interpretation of the chemisorption phenomena, no scaling has been applied. To obtain a qualitative idea of the regions where the C−H, O−H, and C−O stretchings are predicted by the calculations, Table 2, we have used small clusters to analyze isolated fragments.[53] Some of the adsorbed fragments are charged, i.e., OH^-, CH_3O^-, and the computed frequencies can be affected by some uncertainty.

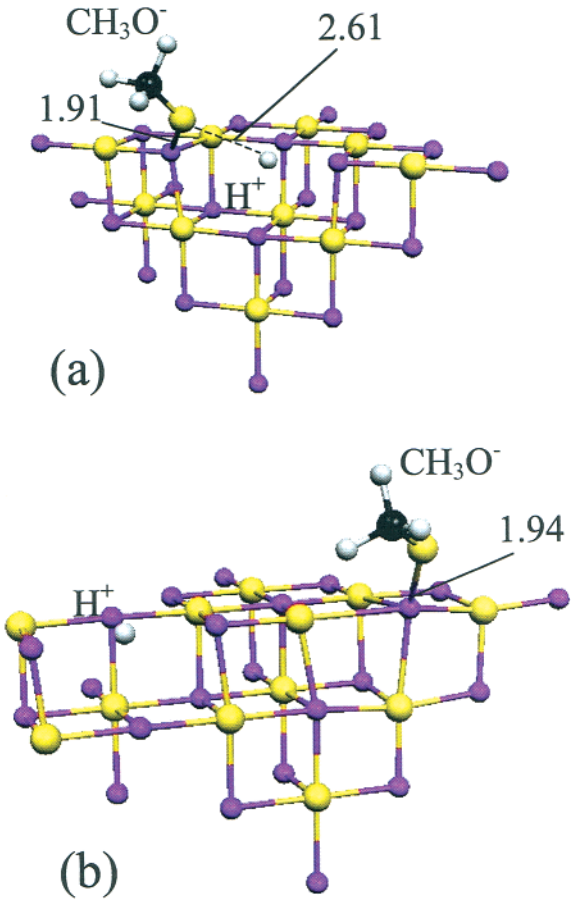

Figure 7. Model of an oxygen vacancy at an edge. (a) Chemisorbed CH_3OH (CH_3O^-−H^+) on [$Mg_{11}O_{10}ECP_{12}$]; (b) dissociated CH_3OH (CH_3O^- + H^+) on [$Mg_{11}O_{10}ECP_{12}$]. For definitions, see Figure 3.

At least three kinds of OH groups can be found in principle on the surface of MgO, one derived from the adsorption of a H^+ ion to a surface O^{2-} anionic site, one due to the adsorption of an OH^- group on a Mg^{2+} cation, and the last one originating from physisorbed CH_3OH. The OH stretchings fall in a range

between 3100 cm^{-1} (physisorbed CH_3OH) and 3700 cm^{-1} (adsorbed OH). The OH frequency for the physisorbed molecule is strongly red-shifted compared to gas phase because of the formation of a hydrogen bond between the H atom of the OH group and one of the oxygen ions of the surface, Figure 3a; this interaction weakens the hydroxyl O−H bond and diminishes the O−H stretching frequency. It is possible, however, that the field created by the point charges around the quantum cluster also contributes to this large red-shift.

The CH stretching, OCH bending, and CO stretching arise from both physisorbed and dissociated molecules.[54] The CH stretching vibrations fall in a range between 2500 and 3100 cm^{-1}. The OCH bending frequencies are in the 1400−1550 cm^{-1} region but their intensity is low; this holds also for OH bending in the regions between 1100 and 1500 cm^{-1}. Intense C−O stretching modes are found between 1090 and 1140 cm^{-1}. This means that the C−O stretching frequency of adsorbed methanol is always blue-shifted compared to the gas phase (1050 cm^{-1}).

The last vibrational mode considered is that of a proton trapped at an F_S center. An H^+ ion has been placed into an oxygen vacancy at a terrace site, $[Mg_5O_{12}ECP_{24}]$, or at an edge site, $[Mg_4O_9ECP_{16}]$. The corresponding frequencies are between 800 and 950 cm^{-1}, Table 2, and are rather intense. The formation of a proton trapped at an F center implies the formation of a chemisorbed CH_3OH species, as shown in Figure 6. This adsorbed species, dissociated into CH_3O^- and H^+, exhibits C−H stretchings around 2800−2900 cm^{-1}, a CH bending at 1480 cm^{-1}, and two strong bands at 1083 and 1030 cm^{-1} due to C−O stretching and to the H vibration in the F center, respectively, see Table 2. The importance of these latter two bands for the interpretation of the FTIR spectra will be further discussed below.

6. Discussion

Experimental TDS and FTIR spectra and computational results can now be compared. The experimental results refer to two different preparation modes of the MgO films, characterized by a different defect density. On both defect-rich and defect-poor films most of adsorbed methanol desorbs for temperatures around 180 K, Figure 1. The calculations have shown that the species which desorb at higher temperatures are clearly related to molecular and dissociative chemisorption at defect sites. The analysis of the IR frequencies provides a tool to better characterize the species formed at the surface.

The two IR bands at 3285 and 3515 cm^{-1} observed at $T =$ 90 K on the films, Figures 1 and 2, are quite similar to those measured at 3330 and 3600 cm^{-1} on polycrystalline MgO[5] or on MgO films.[12] The broad band at 3285 cm^{-1}, Figure 2, completely disappears at 180 K, as it is due to multilayer and physisorbed methanol. In the calculations, ν(OH) for physisorbed CH_3OH is at 3100 cm^{-1}, i.e., 200 cm^{-1} lower than the experimental value. This is partly due to the shortcuts of the calculations. However, one should keep in mind that at high coverages the actual structure of the physisorbed molecule is determined by adsorbate−adsorbate interactions more than by adsorbate−substrate bonding, and that dipole−dipole coupling effects can result in considerable shifts of the gas-phase monomer frequencies.

The feature at 3515 cm^{-1}, due to OH groups from chemisorbed or dissociatively adsorption methanol, remains up to T = 180 K but disappears completely for temperatures above 200 K. This is true for both defect-rich and defect-poor films. In the calculations vibrations from surface OH groups fall in around 3700 cm^{-1} (here the difference between theory and experiments is largely due to the harmonic approximation). The IR spectra for temperatures above 200 K seems to indicate that the films are completely dehydroxylated.

The peaks at about 2800−2900 cm^{-1} are due to the C−H stretching of the CH_3O^- fragments (the formation of CH_3 methyl groups seems to be unfavorable from the calculated energies). Similar bands have been observed on MgO powders;[5] on the MgO films a feature at around 2930 cm^{-1}, attributed to a methoxy group, is stable up to 500 K on the defect-rich film. In the calculations the C−H modes are found in a wide region between 2500 and 3100 cm^{-1}. A band at 1475 cm^{-1} (insert of Figure 1) of low intensity is completely suppressed at 180 K (not shown in Figure 2) and arises from bending vibrations of the CH_3 groups. Similar bands have been observed at 1458 and 1423 cm^{-1} in polycrystalline MgO[5] and at 1437 cm^{-1} on MgO films,[12] respectively.

Very important for the present analysis is the peak at about 1100 cm^{-1}. This is clearly the convolution of various bands. One dominant contribution to this region is the C−O stretching mode (1034 cm^{-1} in the free molecule). In polycrystalline MgO, two bands at 1114 and 1068 cm^{-1} due to this mode show a considerable dependence of the intensity on methanol concentration.[5] In Goodman's study, a not-well-resolved feature at 1143 cm^{-1} has been observed.[12] On the defect-poor MgO thin films, Figure 2, the position of the maximum changes by increasing the temperature; while two well-resolved peaks are seen at 1050 and 1080 cm^{-1} at $T = 90$ K, only one peak at 1119 cm^{-1} remains for temperatures around 230 K but the intensity is greatly attenuated. This peak is nearly absent above RT. This analysis is also consistent with XPS C(1s) measurements of methanol adsorbed on MgO films[6] which indicate that surface methoxide species are formed between 180 and 300 K. Notice that all the reported values are blue-shifted with respect to gas-phase methanol, as found theoretically for this stretching mode. This suggests that the bands around 1100 cm^{-1} in the defect-poor films are *entirely* due to C−O stretching modes. Things are different on the defect-rich films. Here, in fact, the band around 1100 cm^{-1} shows a similar shift and intensity change by raising the temperature as for the defect-poor films (the maximum moves from 1050 cm^{-1} at 90 K to 1120 cm^{-1} at 200 K); however, for temperatures as high as 560 K, a signal is still found around 1070 cm^{-1} despite the fact that all the methanol has desorbed from the surface. This is shown (1) by the TDS of Figure 1 and (2) by the IR spectra, which show no presence of C−H bond stretching at temperatures where the 1070 cm^{-1} band is still present.

Therefore, the band at 1070 cm^{-1} must arise from a species different from C−O, highly stable on the surface (it disappears only above 600 K). Previous work has shown that oxygen vacancies are present on defect-rich films.[14] These defect centers determine to a large extent the chemistry of the MgO films. Our calculations show that F centers easily dissociate methanol, giving a CH_3O^- group and an H^+ ion adsorbed into the F center. The CH_3O^- fragment is expected to diffuse on the surface and eventually desorb as the temperature is increased. The proton adsorbed in the vacancy is strongly bound as the dissociation of a neutral H atom, $F_s/H^+ \rightarrow F_s^+ + H^\bullet$, costs 4.1 eV. This represents a crude estimate of the barrier to overcome in order to observe H_2 desorption from the surface. Once the H atom is detached from the F_s center, it will rapidly diffuse on the surface. In fact, the binding of an H atom to an O_{5c} ion on a terrace is of about 0.5 eV. Diffusion will eventually lead to recombination

with a second H to form H_2; H_2 is weakly bound to the MgO terrace sites and at 580 K will immediately desorb.

The hydrogen adsorbed in the F center gives rise to vibrations of strong intensity at 830−950 cm^{-1} when is isolated, and to an intense band at 1030 cm^{-1} in the chemisorbed complex shown in Figure 6, see also Table 2. Keeping in mind the approximations of the model (only partial relaxation of the cluster is allowed), it is tempting to assign the stable species which gives rise to this band to H atoms incorporated into oxygen vacancies. Another indirect support for the assignment of the 1070 cm^{-1} band to a trapped proton at a neutral vacancy (formally H^-) comes from IR studies of adsorbed H_2 on MgO powders. H_2 dissociates heterolytically on MgO, forming an adsorbed proton, H^+, and a hydride, H^{-1},[55] with well-characterized frequencies at 3712 and 1130 cm^{-1}, respectively.[43,44] While it is likely that the sites involved in the two processes are different,[56] it is interesting to note that hydride species absorb in the same spectral region found in the present experiments.

7. Conclusions

The experimental−theoretical study of methanol adsorbed on MgO films with different defect density allows us to make some proposals for the surface sites responsible for the MgO reactivity. On the inert terrace sites, only physisorption is observed. Molecular chemisorption, activation, and heterolytic dissociation occur on irregular sites. The low-coordinated Mg−O pairs of ions located at edges and steps can lead to strongly activated and even dissociated methanol molecules. Adsorption of CH_3O^- and H^+ fragments seems to be preferred over dissociation into CH_3^+ and OH^- units. All these species are stable on the surface for temperatures up to 350 K and account for the TDS spectra of the defect-poor films. On defect-rich films additional features are found in both TDS and FTIR spectra. H_2 is released for $T = 580$ K from specific defect sites where H atoms are still trapped after all other molecular fragments have been desorbed from the surface. Also on the basis of the ab initio cluster calculations, we propose that these hydrogen atoms are bound to oxygen vacancy centers present on the defect-rich MgO films.

Acknowledgment. This work has been supported by Italian INFM, PRA ISADORA project, Italian Ministry of University and Research (MIUR), PRIN project, University of Ulm, HBFG-Grant (182-349). S. Abbet is supported by a postdoctoral fellowship of the Swiss National Science Foundation. K. Judai thanks the Alexander von Humboldt-Foundation for a fellowship.

References and Notes

(1) Boudard, M.; Delbouile, A.; Derouane, E. G.; Indovina, V.; Walters, A. B. *J. Am. Chem. Soc.* **1972**, *94*, 6622.
(2) Mars, P.; Scholten, J. J.; Zwietering, P. *Adv. Catal.* **1963**, *14*, 35.
(3) Ziolek, M.; Kujawa, J.; Saur, O.; Lavalley, J. C. *J. Phys. Chem.* **1992**, *97*, 9761.
(4) Bensitel, M.; Saur, O.; Lavalley, J. C. *Mater. Chem. Phys.* **1991**, *28* , 309.
(5) Tench, A. J.; Giles, D.; Kibblewhite, J. F. *Trans. Faraday Soc.* **1971**, *67*, 854.
(6) Peng, X. D.; Barteau, J. M. *Langmuir* **1991**, *7*, 1426.
(7) Pacchioni, G. Theory of point defects on ionic oxides. In *Oxide Surfaces, The Chemical Physics of Solid Surfaces*; Woodruff, P., Ed.; Elsevier: Amsterdam, 2001; Vol. 9, pp 94−135.
(8) Heiz, U.; Schneider, W. D. *J. Phys. D: Appl. Phys.* **2000**, *33*, R85.
(9) *Oxide surfaces, The Chemical Physics of Solid Surfaces*; Woodruff, P., Ed.; Elsevier: Amsterdam, 2001; Vol. 9.
(10) Freund, H.-J. *Faraday Discuss.* **1999**, *114*, 1.
(11) Wu, M.-C.; Estrada, C. A.; Goodman, D. W. *Phys. Rev. Lett.* **1991**, *67*, 2910.
(12) Wu, M.-C.; Estrada, C. A.; Corneille, J. S.; Goodman, D. W. *J. Chem. Phys.* **1992**, *96*, 3892.
(13) Günster, J.; Liu, G.; Stultz, J.; Goodman, D. W. *J. Chem. Phys.* **1999**, *110*, 2558.
(14) Abbet, S.; Riedo, E.; Brune, H.; Heiz, U.; Ferrari, A. M.; Giordano, L.; Pacchioni, G. *J. Am. Chem. Soc.* **2001**, *123*, 6172.
(15) Lopez, N.; Illas, F.; Pacchioni, G. *J. Am. Chem. Soc.* **1999**, *121*, 813.
(16) Paganini, M.; Chiesa, M.; Giamello, E.; Coluccia, S.; Murphy, D. M.; Pacchioni, G. *Surf. Sci.* **1999**, *421*, 246.
(17) Ferrari, A. M.; Pacchioni, G. *J. Phys. Chem.* **1995**, *99*, 17010.
(18) Heiz, U.; Vanolli, F.; Trento, L.; Schneider, W.-D. *Rev. Sci. Instrum.* **1997**, *68*, 1986.
(19) Schaffner, M.-H.; Patthey, F.; Schneider, W.-D. *Surf. Sci.* **1998**, *417*, 159.
(20) Wu, M.-C.; Corneille, J. S.; He, J.-W.; Estrada, C. A.; Goodman, D. W. *J. Vac. Sci. Technol. A* **1992**, *10*, 1467.
(21) Wu, M.-C.; Corneille, J. S.; Estrada, C. A.; He, J.-W.; Goodman, W. D. *Chem. Phys. Lett.* **1991**, *182*, 472.
(22) Liehr, M.; Thiry, P. A.; Pireaux, J. J.; Caudano, R.; *Phys. Rev. B* **1986**, *33*, 5682.
(23) Tjeng, L. H.; Vos, A. R.; Sawatzky, G. A. *Surf. Sci.* **1990**, *235*, 269.
(24) He, J. W.; Møller, P. L. *Chem. Phys. Lett.* **1986**, *129*, 13.
(25) Nygren, M. A.; Petterson, L. G. M. *J. Chem. Phys.* **1996**, *105*, 9339.
(26) He, J. W.; Cesar, A. E.; Corneille, J. S.; Wu, M.-C.; Goodman, D. W. *Surf. Sci.* **1992**, *261*, 167.
(27) Wichtendahl, R.; Rodriguez-Rodrigo, R.; Härtel, U.; Kuhlenbeck, H.; Freund, H. J. *Surf. Sci.* **1999**, *423*, 90.
(28) Wichtendahl, R.; Rodriguez-Rodrigo, R.; Härtel, U.; Kuhlenbeck, H.; Freund, H. J. *Phys. Stat. Sol. (a)* **1999**, *173*, 93.
(29) Pacchioni, G.; Ferrari, A. M.; Marquez, A. M.; Illas, F. *J. Comput. Chem.* **1997**, *18*, 617.
(30) Cundari, T. R.; Stevens, W. J. *J. Chem. Phys.* **1993**, *98*, 5555.
(31) Stevens, W. J.; Basch, H.; Krauss, M. J. *J. Chem. Phys.* **1984**, *81*, 6026.
(32) Winter, N. W.; Pitzer, R. M. *J. Chem. Phys.* **1988**, *89*, 89.
(33) Nygren, M. A.; Petterson, L. G. M.; Barandiaran, Z.; Seijo, L. *J. Chem. Phys.* **1994**, *100*, 2010.
(34) Mejias, J. A.; Marquez, A. M.; Fernandez Sanz, J.; Fernandez-Garcia, M.; Ricart, J. M.; Sousa, C.; Illas, F. *Surf. Sci.* **1995**, *327*, 59.
(35) Ferrari, A. M.; Soave, R.; D'Ercole, A.; Pisani, C.; Giamello, E.; Pacchioni, G. *Surf. Sci.* **2001**, *479*, 83.
(36) Pacchioni, G. *Surf. Rev. Lett.* **2000**, *7*, 277.
(37) Becke, A. D. *J. Chem. Phys.* **1993**, *98*, 5648.
(38) Lee, C.; Yang, W.; Parr, R. G. *Phys. Rev. B* **1988**, *37*, 785.
(39) Koch, W.; Holthausen, M. C. A Chemist's Guide to Density Functional Theory; Wiley-VCH: Weinheim, 2002.
(40) Hehre, W. J.; Ditchfield, R.; Pople, J. A. *J. Chem. Phys.* **1972**, *56*, 2257.
(41) Boys, S. F.; Bernardi, F. *Mol. Phys.* **1970**, *19*, 553.
(42) Frisch, M. J., et al. *Gaussian 98*; Gaussian Inc.: Pittsburgh, PA, 1997.
(43) Coluccia, S.; Boccuzzi, F.; Ghiotti, G.; Morterra, C. *J. Chem. Soc., Faraday Trans. 1* **1982**, *78*, 2111.
(44) Diwald, O.; Hofmann, P.; Knozinger, E. *Phys. Chem. Chem. Phys.* **1999**, *1*, 713.
(45) Brown, G. E., et al. *Chem. Rev.* **1999**, *99*, 77, and references therein.
(46) Giordano, L.; Goniakovski, J.; Suzanne, J. *Phys. Rev. Lett.* **1998**, *81*, 1271.
(47) Kim, Y. D.; Stulz, J.; Goodman, D. W. *J. Phys. Chem. B* **2002**, *106*, 1515.
(48) Branda, M. M.; Peralta, J. E.; Castellani, N. J.; Contreras, R. H. *Surf. Sci.* **2002**, *504*, 235.
(49) Anchell, J. L.; Hess, A. C. *J. Phys. Chem.* **1996**, *100*, 18317.
(50) Rodriguez, J. A.; Maiti, A. *J. Phys. Chem. B* **2000**, *104*, 3630.
(51) Pacchioni, G.; Pescarmona, P. *Surf. Sci.* **1998**, *412/413*, 657.
(52) Herzberg, G. *Molecular Spectran and Molecular Structure, III. Electronic Spectra and Electronic Structure of Polyatomic Molecules*; Van Nostrand: New York, 1966.
(53) We have modeled these three situations by adding H^+ on the oxygen-centered [$Mg_5O_5ECP_{12}$] terrace or [Mg_4O_1] edge clusters, or an OH^- on the magnesium-centered [$Mg_5O_5ECP_9$] terrace or [$Mg_1O_4ECP_9$] edge clusters; the frequency of physisorbed methanol has been evaluated by using the [$Mg_8O_8ECP_{14}$] terrace cluster.
(54) CH_3O^- has been adsorbed on a [$Mg_1O_5ECP_{13}$] model of a terrace site, on a [$Mg_1O_4ECP_9$] model of an edge, and on a [$Mg_2O_8ECP_{18}$] model of a step. CH_3^+ has been adsorbed on a [Mg_5O_1] and [Mg_4O_1] minimal models of terrace and edge anions, respectively.
(55) Tench, A. J. *Surf. Sci.* **1971**, *25*, 625.
(56) Ricci, D.; Di Valentin, C.; Pacchioni, G.; Sushko, P.; Shluger, A.; Giamello, E. To be published.